Supplementary Figure S1

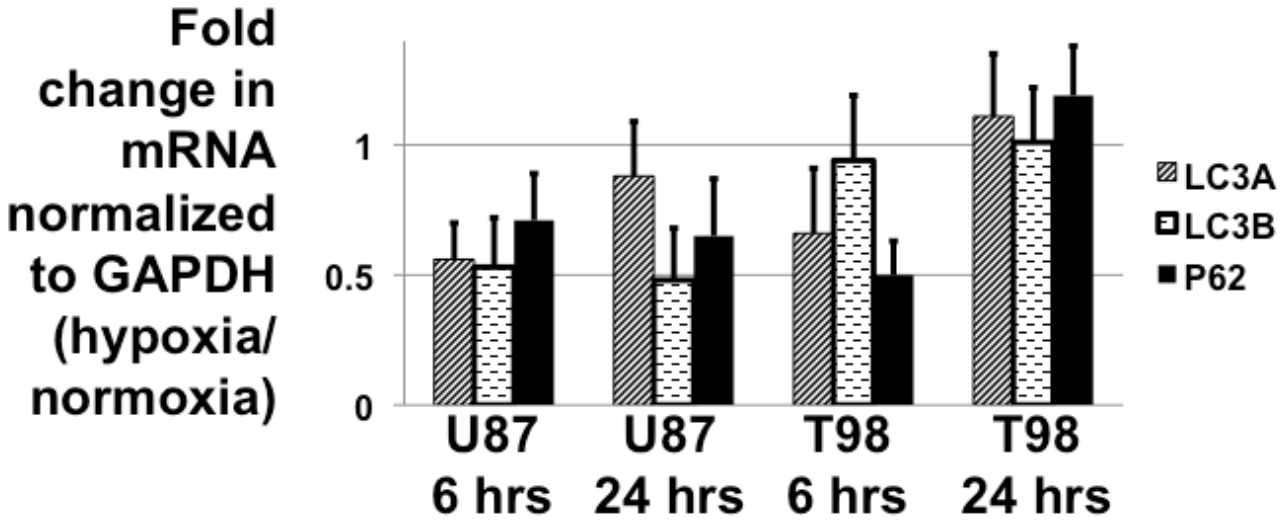

Supplementary Figure S1. Real time RT-PCR measuring autophagy-related transcripts of U87MG and T98G glioma cells in hypoxia relative to normoxia. Shown are fold change in the levels of LC3A, LC3B, and p62 transcripts after normalization relative to GAPDH in hypoxia relative to normoxia for 6 and 24 hours in U87MG and T98G cells. Error bars represent standard deviations.

Supplementary Figure S2

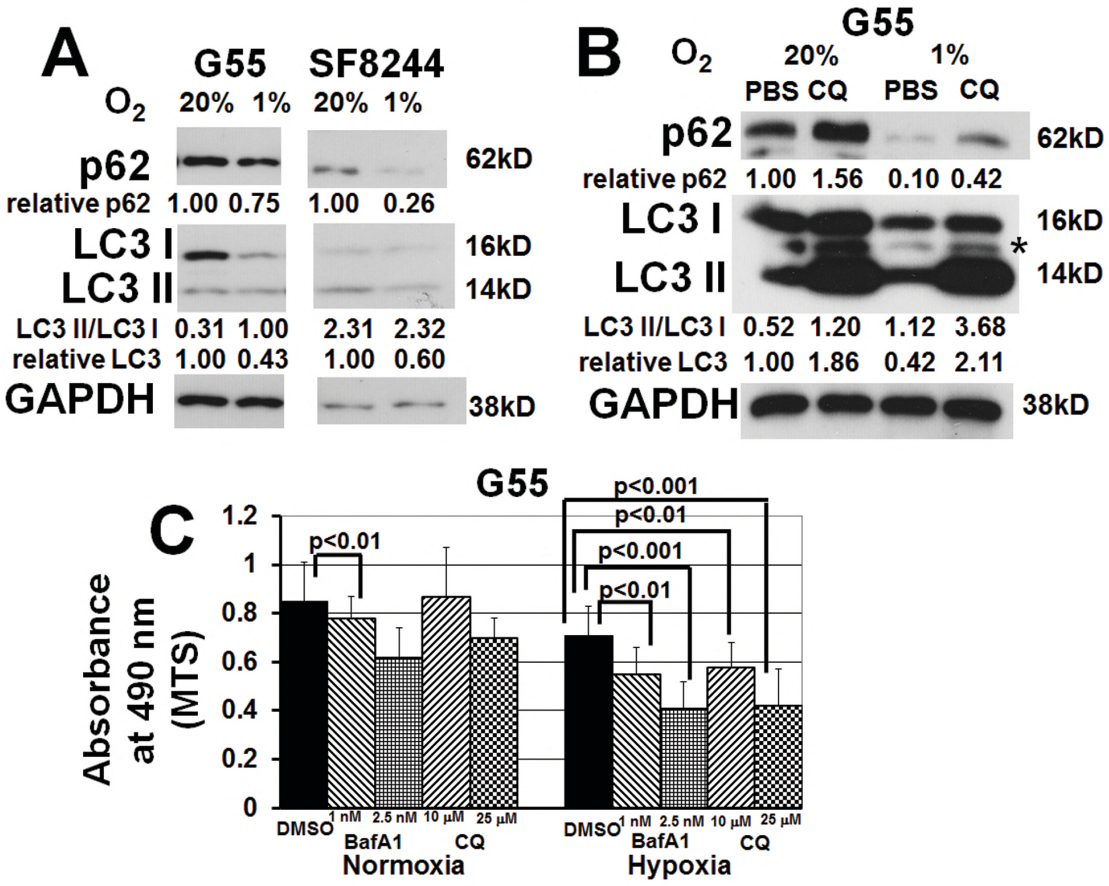

Supplementary Figure S2. Hypoxia-induced autophagy in cultured G55 and SF8244 cells and effects of chloroquine on cultured cells. (A) G55 and SF8244 cells in hypoxia (1% oxygen) for 24 hours exhibited increased, relative to normoxia (20% oxygen), degradation of p62. G55 cells exhibited increased conversion of LC3-I to LC3-II in hypoxia, while SF8244 cells exhibited overall degradation of total LC3 in hypoxia. (B) After 24 hours, late autophagy inhibitor chloroquine (CQ; 10 μM) blocked hypoxia-induced p62 degradation, and caused more LC3-I to LC3-II conversion to occur. * indicates a nonspecific band. (C) After 72 hours, while 10 and 25 μM chloroquine did not change normoxic G55 cell survival, these concentrations decreased hypoxic G55 cell survival (relative to normoxia) in a chloroquine dose-dependent manner ($P<0.05$). Similar effects were noted after 72 hours of treatment with Bafilomycin A1 (BafA1), also a late autophagy inhibitor.

Supplementary Figure S3

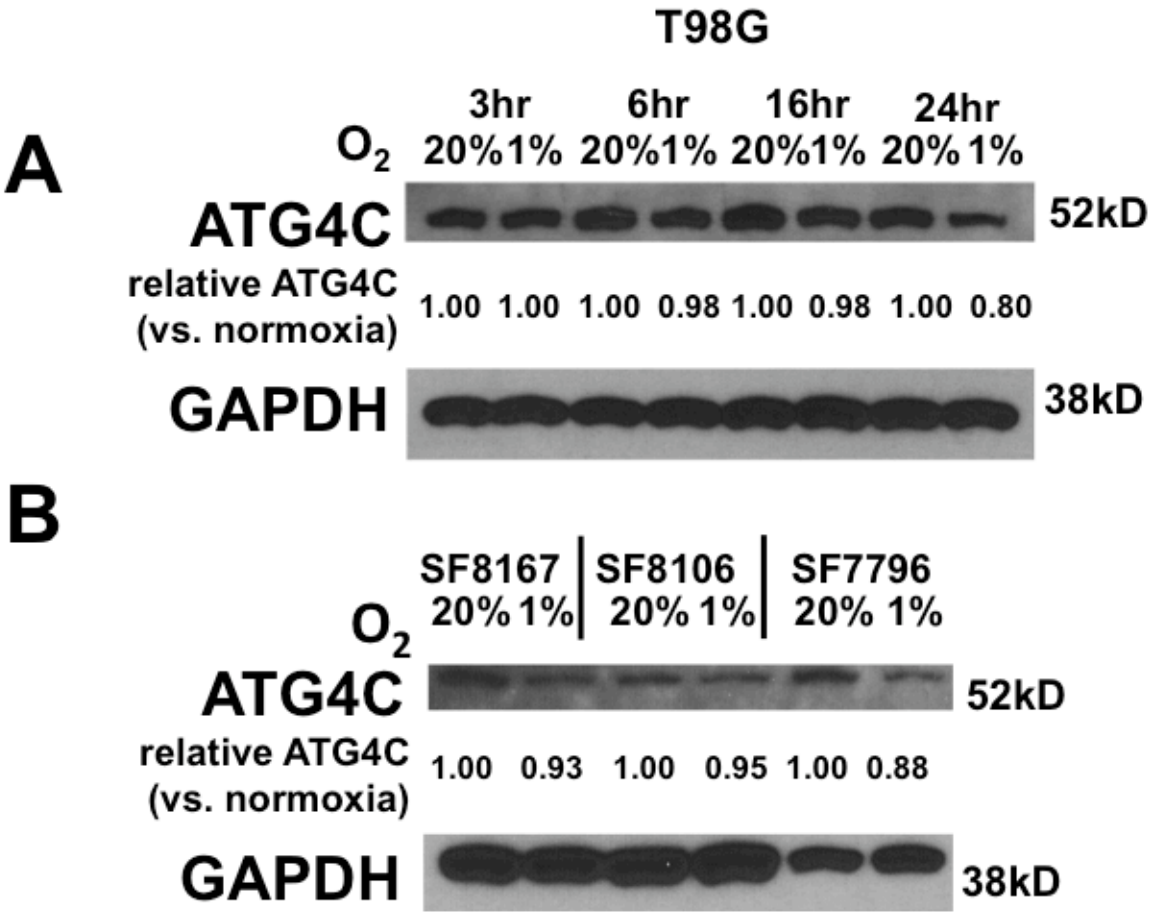

Supplementary Figure S3. Effect of hypoxia on ATG4C expression in cultured human glioma cells. (A) T98G human glioma cell line cultured for 3, 6, 16, and 24 hours at normoxia (20% oxygen) and hypoxia (1% oxygen) exhibited decreased expression of the ATG4C protease at hypoxia relative to normoxia. (B) Primary human glioma cells SF8167, SF8106, and SF7796 exhibited decreased expression of the ATG4C protease in hypoxia (1% oxygen) relative to normoxia (20% oxygen) after 24 hours of being cultured.

Supplementary Figure S4

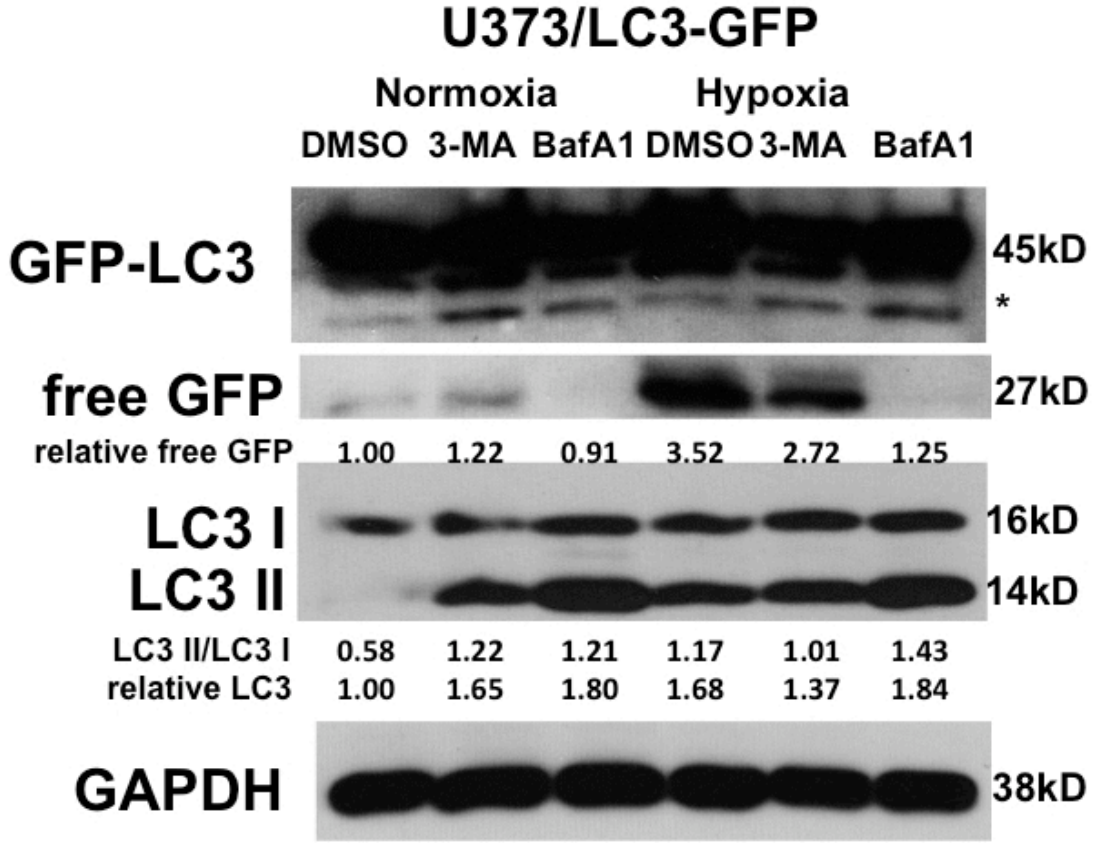

Supplementary Figure S4. Western blot markers of autophagy in hypoxic U373/GFP-LC3 cells. Western blotting revealed increased free GFP in hypoxic versus normoxic U373/GFP cells, with 3-MA and BafA1 lowering the amount of free GFP in hypoxic cells. As with U87MG cells, the ratio of LC3-II to LC3-I increased with hypoxia and 3-MA inhibited conversion of LC3-I to LC3-II, while BafA1 caused more LC3-I to LC3-II conversion to occur, although the inhibitor effects were less than seen with U87MG cells in Figure 3A. * indicates a nonspecific band.

Supplementary Figure S5

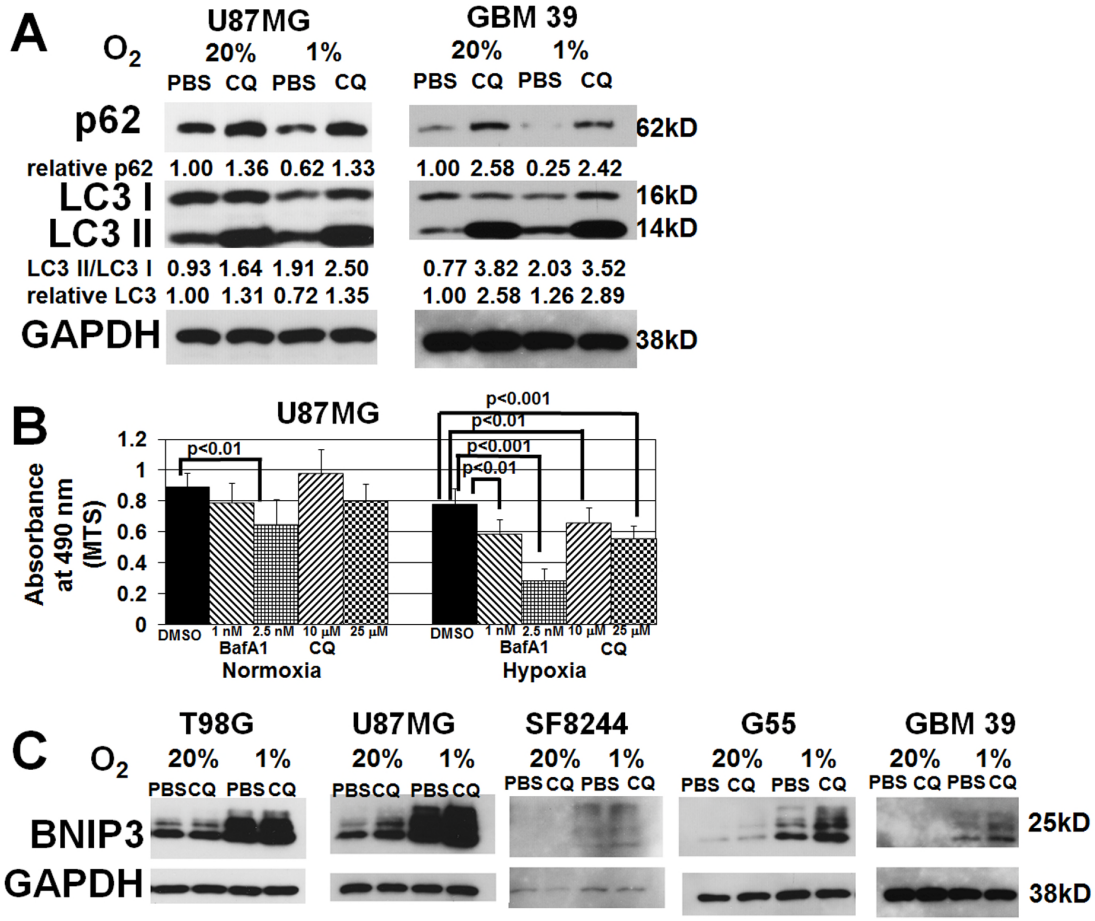

Supplementary Figure S5. Autophagy inhibitor chloroquine inhibits hypoxia-induced autophagy and reduces cell survival, without altering BNIP3 expression *in vitro*. (A) After 24 hours, late autophagy inhibitor chloroquine (CQ; 10 μM) blocked hypoxia-induced p62 degradation, and increased LC3-I to LC3-II conversion. (B) After 72 hours, while 10 and 25 μM chloroquine did not change normoxic U87MG cell survival, these concentrations decreased hypoxic U87MG cell survival (relative to normoxia) in a chloroquine dose-dependent manner ($P<0.05$). Similar effects were noted after 72 hours of treatment with Bafilomycin A1 (BafA1), also a late autophagy inhibitor. (C) While hypoxia upregulated BNIP3 expression after 24 hours in 5 different glioma cells (T98G, U87MG, SF8244, G55, and GBM39), chloroquine minimally affected BNIP3 expression.

Supplementary Figure S6

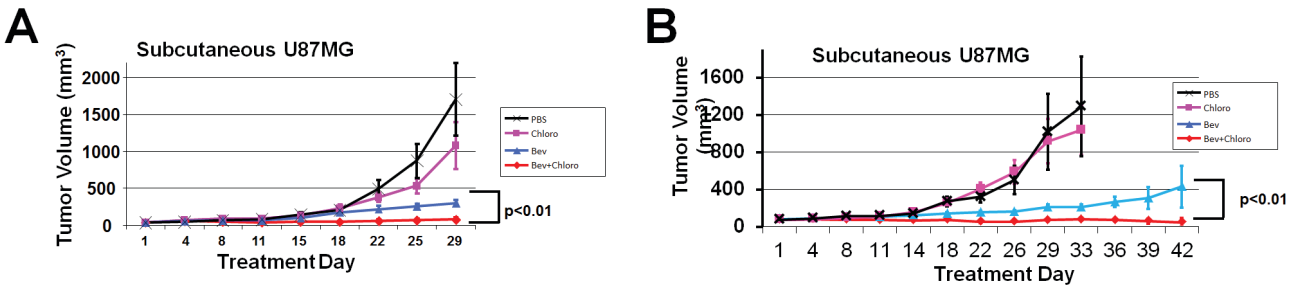

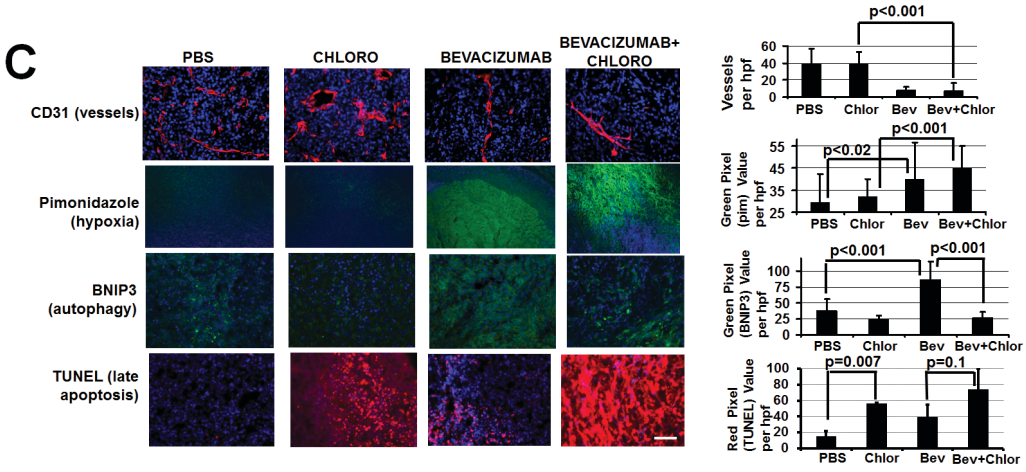

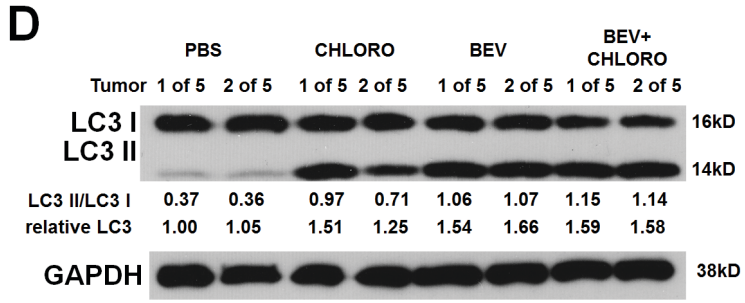

Supplementary Figure S6. Autophagy inhibitor chloroquine combined with angiogenesis inhibitor bevacizumab inhibits U87MG tumor growth *in vivo*. (A) Subcutaneous U87MG tumors in athymic mice were treated with PBS, chloroquine, bevacizumab, or chloroquine combined with bevacizumab. After 4 weeks of treatment, there was significantly different tumor volumes amongst groups ($P<0.005$). Compared to PBS (black curve), chloroquine monotherapy (pink curve) did not inhibit tumor growth ($P>0.05$), while bevacizumab monotherapy (blue curve) inhibited tumor growth ($P<0.05$). Combined therapy with bevacizumab and chloroquine (red curve) inhibited tumor growth ($P<0.01$ combined therapy vs. bevacizumab; $P<0.005$ combined therapy vs. chloroquine). (B) In a repeat of the experiment shown in (A) in which treatment continued after PBS- and chloroquine-treated mice had to be euthanized, differences in volume between bevacizumab versus bevacizumab plus chloroquine treated U87MG tumors were increased over an additional 2 weeks, during which bevacizumab-treated tumors exhibited increased rate of growth while tumors treated with bevacizumab plus chloroquine remained growth suppressed ($P<0.01$). Error bars represent standard errors of the mean, 5 tumors per group. (C) U87MG tumors in each treatment group were analyzed by immunohistochemistry. Vessel density (CD31 staining, red) was decreased in bevacizumab-treated tumors ($P<0.001$). Hypoxia (assessed by treating mice with pimonidazole prior to euthanasia and immunostaining for the adducts that pimonidazole forms in hypoxic areas, green) was increased in all bevacizumab-treated tumors ($P<0.001$). BNIP3 expression (green) was increased by bevacizumab treatment,

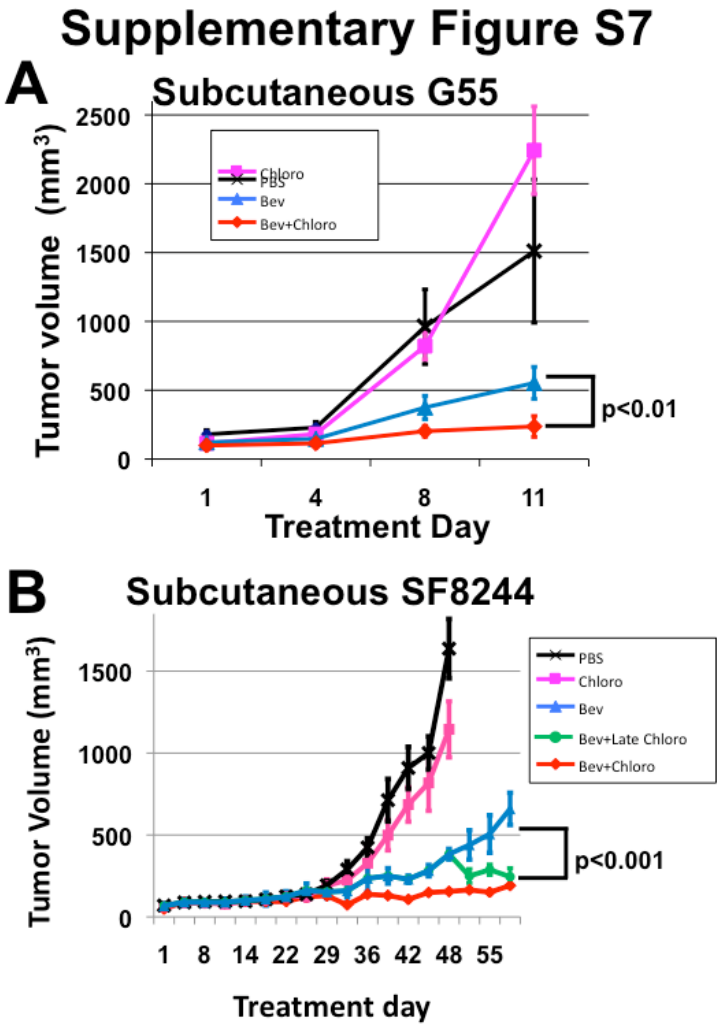

Supplementary Figure S7. Autophagy inhibitor chloroquine combined with angiogenesis inhibitor bevacizumab inhibits subcutaneous tumor growth *in vivo*. (A) Subcutaneous G55 cell line-derived xenografts treated with PBS, chloroquine, bevacizumab, and bevacizumab plus chloroquine exhibited suppressed growth in bevacizumab plus chloroquine treated tumors compared to tumors treated with bevacizumab alone (P<0.01). (B) Subcutaneous xenografts derived from primary SF8244 glioma cells treated with PBS, chloroquine, bevacizumab, or bevacizumab+chloroquine exhibited suppressed growth when treated with bevacizumab+chloroquine relative to bevacizumab monotherapy (P<0.001 for both xenografts). Delayed addition of chloroquine to bevacizumab-treated SF8244 xenografts averaging 400 mm^3 led to growth suppression compared to xenografts continuing to receive bevacizumab monotherapy (P<0.001).

Supplementary Figure S8

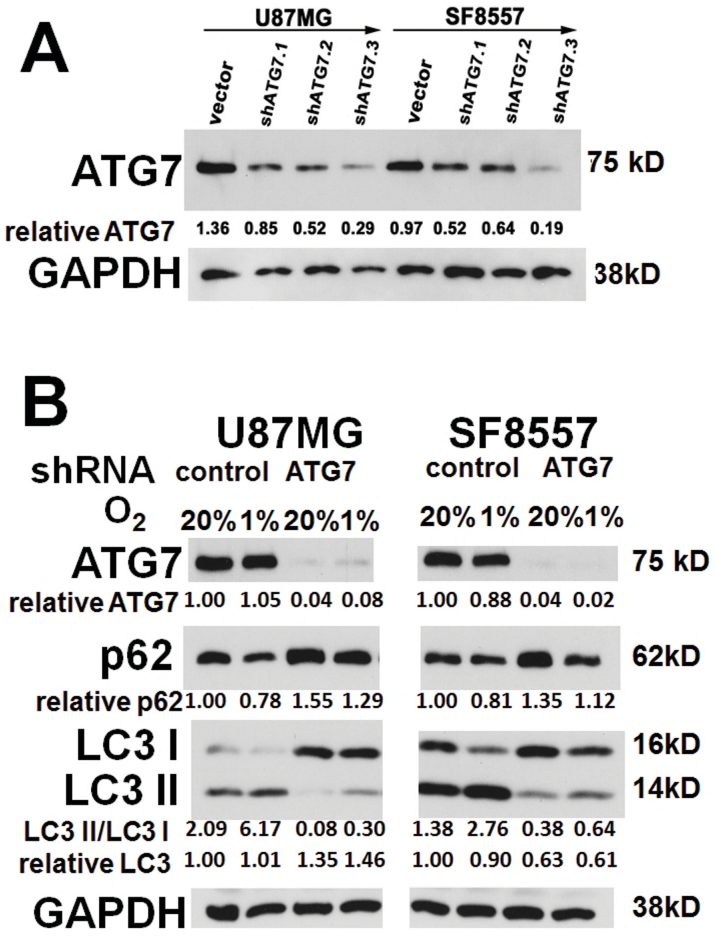

Supplementary Figure S8. Characterizing tumor cells exhibiting knockdown of the ATG autophagy-mediating gene. (A) The U87MG glioma cell line and SF8557 primary glioma cells were transduced to express control vector and 3 different shRNAs targeting ATG7. Western blot revealed the shATG7.3 caused greater ATG7 knockdown than shATG7.2 and shATG7.1, so U87MG and SF8557 cells transduced to express shATG7.3 were selected for further study along with cells transduced with control vector. (B) shATG7.3 blocked the conversion of LC3-I to LC3-II, a marker of autophagy, in U87MG and SF8557 cells exposed to hypoxia for 24 hours.

Supplementary Figure S9

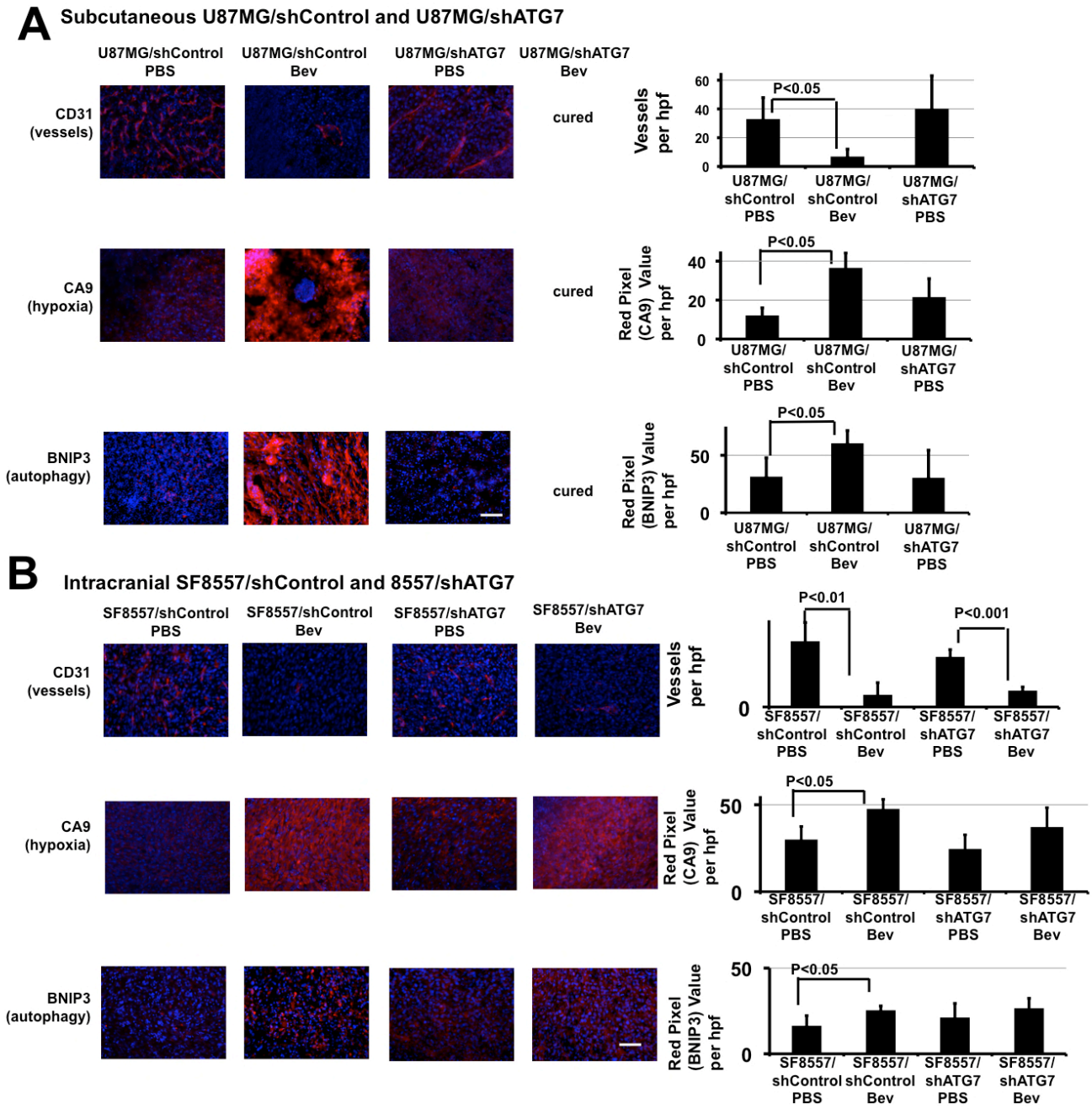

Supplementary Figure S9. Immunostaining of subcutaneous and intracranial tumors derived from cells transduced to express shRNA targeting essential autophagy gene ATG7. Shown are immunostainings (red) of CD31, CA9, and BNIP3 in (A) subcutaneous xenografts derived from shRNA-transduced U87MG cells and (B) intracranial xenografts derived from shRNA-transduced SF8557 cells, after treatment with PBS or bevacizumab. (A) Bevacizumab treatment cured subcutaneous U87/shATG7 xenografts, leaving 3 treatment groups to analyze by immunohistochemistry, which showed that bevacizumab treatment decreased vessel density (CD31), increased hypoxia (CA9), and increased BNIP3 (red) expression ($P<0.05$). (B) Bevacizumab reduced vessel density in intracranial SF8557/shControl and SF8557/shATG7 xenografts ($P<0.01$), increased hypoxia in intracranial SF8557/shControl xenografts ($P<0.05$), and increased BNIP3 expression in intracranial SF8557/shControl xenografts ($P<0.05$). Views shown are 20x. Scale bar, 200 μm.